Scanning Electrochemical Microscopy in Combination with Piezoelectric Quartz Crystal Impedance Analysis for Studying the Growth and Electrochemistry as Well as Microetching of Poly(*o*-phenylenediamine) Thin Films

Xinman Tu,[†] Qingji Xie,*[,†,‡] Canhui Xiang,[‡] Youyu Zhang,[†] and Shouzhuo Yao[†]

Key Laboratory of Chemical Biology and Traditional Chinese Medicine Research (Hunan Normal University), Ministry of Education, Hunan Normal University, Changsha 410081, People's Republic of China, and College of Chemistry and Molecular Sciences, Wuhan University, Wuhan 430072, People's Republic of China

Received: November 18, 2004

The combination of scanning electrochemical microscopy (SECM) with piezoelectric quartz crystal impedance (PQCI) analysis was proposed as a novel multiparameter method for investigating the cyclic voltammetric growth of poly(*o*-phenylenediamine) (P*o*PD) thin films at Au electrodes in aqueous solutions of various pH values and the potentiostatic microetching (localized degradation) of these films in 0.10 mol/L aqueous H_2SO_4 for comparative examinations on polymer porosity and stability. Two potential-sweep ranges, −0.4 to 0.9 (I) and 0 to 0.9 (II) V versus SCE, and four solutions, acidic (A, 0.20 mol/L H_2SO_4 + 0.10 mol/L Na_2SO_4; B, 0.10 mol/L H_2SO_4 + 0.20 mol/L Na_2SO_4), neutral (C, 0.10 mol/L PBS + 0.20 mol/L Na_2SO_4, pH 7.2), and alkaline (D, 0.20 mol/L NaOH + 0.20 mol/L Na_2SO_4) aqueous solutions, were selected for P*o*PD growth. The pH increase for the polymerization solution increased the molar percentage of polyaniline-like chains in P*o*PD, as quantified from the current peaks at ∼0.6 V versus a saturated calomel electrode (SCE) for the oxidation of $-NH_2$ groups in as-prepared P*o*PD (grown from solutions C and D) during their redox switching in 0.10 mol/L aqueous H_2SO_4 for the first time. The unusual PQCI responses observed at negative potentials (potential range I) in the first several potential cycles during the cyclic voltammetric growth of P*o*PD in acidic and neutral solutions have been reasonably explained as being due to the precipitation/dissolution of the poorly soluble phenazinehydrine charge-transfer complexes developed during redox switching of oligomers for the first time, which brought about much less compact P*o*PD films and their higher degradability than those grown in the same solution but over potential range II. SECM, scanning electron microscopy (SEM), and piezoelectric quartz crystal (PQC) frequency were used to estimate the sizes of etched microscale spots. In addition, the *x*-, *y*-, or *z*-axis movement of a Pt microelectrode of 25-μm diameter near the PQC electrode was found to influence negligibly the PQCI responses in 1.0 mol/L aqueous Na_2SO_4 containing $K_4Fe(CN)_6$ up to 0.10 mol/L, and a new protocol of dynamically electrodepositing silver microwires via the chemical-lens method was proposed for examining the local mass-sensitivity distribution on the PQC surface.

1. Introduction

Poly(*o*-phenylenediamine) (P*o*PD) has attracted much attention in biosensor development,[1−4] electrocatalysis,[5,6] and corrosion inhibition[7] and as electrochromic materials.[8] More recently, molecularly imprinted films based on P*o*PD have been prepared for developing chemo/biosensors.[9−11] However, the polymer chain structure for P*o*PD is strongly dependent on the polymerization conditions and is not very well understood at present, and both the polyaniline-like chains and the ladder structure with phenazine units have been reported,[12−15] as shown in Chart 1. Therefore, structure−property research of P*o*PD films may be of fundamental importance toward their increasing applications.

The combination of the piezoelectric quartz crystal impedance (PQCI) analysis method with a dc or ac electrochemical technique, being a multiple-parameter electrochemical quartz crystal microbalance (EQCM), can characterize the piezoelectric quartz crystal (PQC) resonance very completely and provide multidimensional piezoelectric information simultaneously during an electrochemical perturbation.[16−25] Generally, the electroacoustic impedance of the PQC resonance is analyzed on the basis of a Butterworth−van Dyke (BVD) equivalent electrical circuit, which consists of a motional arm and a static arm in parallel. The motional arm contains three equivalent circuit elements in series, that is, the motional resistance (R_1), the motional inductance (L_1), and the motional capacitance (C_1). The static arm contains only the static capacitance (C_0). Each equivalent circuit parameter has its distinct physical meaning.[16−25]

CHART 1: Chemical Structures of Poly(*o*-phenylenediamine)

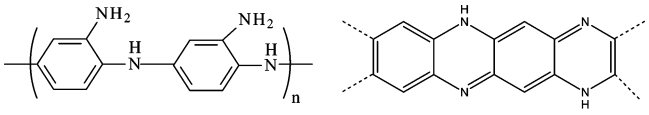

Polyaniline-like structure Ladder structure with phenazine units

The Sauerbrey equation has been used to calculate the change of electrode mass that results from the deposition and dissolution of a rigid, thin, and homogeneous film[26]

$$\Delta f_0 = -2.264 \times 10^{-6} f_{0g}^{\ 2} \Delta m/A \qquad (1)$$

* Corresponding author. E-mail: xieqj@hunnu.edu.cn.
† Hunan Normal University.
‡ Wuhan University.

10.1021/jp044731n CCC: $30.25
Published on Web 02/12/2005

where Δf_0 is the frequency shift in hertz, f_{0g} is the fundamental frequency of the unperturbed crystal in hertz, Δm is the mass change in grams, and A is the piezoelectrically active area of electrode in square centimeters.

The EQCM is also sensitive to the density and viscosity of the solution near the EQCM electrode surface,[17,18,23] and a net liquid-loading effect for a PQC with one side contacting solution can be characterized by the following equation[19,21−25]

$$2\pi L_{1q}\delta\Delta f_{G1/2L} \approx \Delta R_{1L} = 2\pi f \Delta L_{1L} = -4\pi L_{1q}\Delta f_{0L}\sqrt{f\mu_q}/\sqrt{f_{0g}\bar{c}_{66}} \approx -4\pi L_{1q}\Delta f_{0L} \quad (2)$$

where $\delta\Delta f_{G1/2L}$, Δf_{0L}, ΔR_{1L}, and ΔL_{1L} are the changes in $\Delta f_{G1/2}$ (the half peak width of the conductance curve), f_0 (the resonant frequency, and $f_0 = 1/[2\pi(L_1C_1)^{1/2}]$), R_1, and L_1 due to variations of the solution density and viscosity, respectively, f_{0g} is the resonant frequency in air, μ_q (2.947×10^{10} N m^{-2}) is the shear modulus for the AT-cut quartz, L_{1q} is the motional inductance for the PQC in air, and $\bar{c}_{66}$ (2.957×10^{10} N m^{-2}) is the lossy piezoelectrically stiffened quartz elastic constant.[19,21−25]

According to eq 2, the characteristic values of $\Delta f_{0L}/\Delta R_{1L}$ and $\Delta f_{0L}/\delta\Delta f_{G1/2L}$ for a net viscous effect on the 9-MHz PQC resonance are ~ -10 Hz Ω^{-1} and -0.50, respectively. Obviously, for an investigated system, the larger the absolute values of $\Delta f_0/\Delta R_1$ and $\Delta f_0/\delta\Delta f_{G1/2}$, the weaker the viscous effect and the stronger the mass effect reflected by the Sauerbrey equation.

Scanning electrochemical microscopy (SECM) usually works in the bipotentiostat mode, with a micrometer or submicrometer ultra-microelectrode (UME, working electrode no. 1) scanned along the *x*-, *y*-, or *z*-axis over a conducting (working electrode no. 2) or insulating substrate.[27−30] The UME can be used either as a probe to detect and/or image the localized electrochemical event at the substrate[31,32] or as a localized stimulator to construct a micro- or nanoscale structure (or etch a design) at the substrate. The SECM technique has also been applied for studying the heterogeneous kinetics of chemical reactions at the liquid/solid and liquid/liquid interfaces.[33−35] Moreover, SECM has been introduced as one of the very promising wet etching techniques in modifying metal and semiconductor surfaces.[36−40] However, few attempts have been reported to study etching for polymer.

If the SECM substrate, which is usually motionless, is replaced with a high-frequency-oscillating quartz crystal wafer, the active and passive (UME-induced) electrochemical events at the substrate can be simultaneously detected by the EQCM method, making it feasible to depict a practical electrochemical process in less ambiguity or to improve both the EQCM and SECM methodologies. Several groups have developed such integrated EQCM/SECM methods. The first combination of SECM with EQCM was perhaps reported by Hillier and Ward.[41] The local mass sensitivity above the entire quartz plate was mapped during electrochemical copper deposition, giving an approximate Gaussian distribution. Oyama et al. introduced scanning electrode quartz crystal analysis to investigate the spatial resolution of a quartz crystal microbalance (QCM) by oscillating the crystal in a localized area, controlled by the close approach of a microelectrode within a lateral resolution of 2 mm for a 5-MHz crystal.[42,43] Cliffel and Bard applied the combination method to the tip-induced etching of silver deposits and the electrochemical analysis of C_{60} films.[44] The same group dealt with mass changes caused by the reduction of C_{60} caged in *tert*-butylcalix[8]arene and cast as a particle film onto the EQCM surface.[45] The authors used an UME to probe the macroscopic dissolution of C_{60}^-, as indicated by a simultaneous increase of the resonant frequency by several hundred hertz.

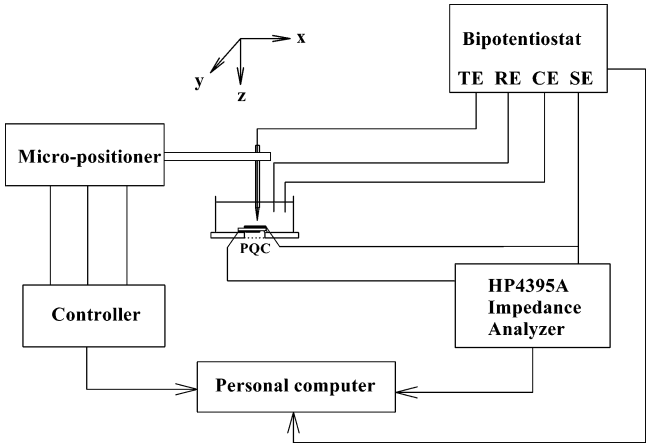

Figure 1. Schematic illustration of the CHI900A scanning electrochemical microscope in combination with the HP4395A impedance analyzer for PQCI analysis. See text for details.

Recently, Hess and co-workers have also applied this EQCM/SECM combination method to perform laterally and vertically resolved frequency measurements in the presence and absence of surface modifying processes.[46] Gollas et al. introduced a new EQCM/SECM combination method to study the Cu (II/I/0) system via rapid in situ measurement of the modulus of the quartz crystal's transfer function.[47]

In this work, we introduce a new combination of SECM with PQCI analysis as a multiparameter method for studying the cyclic voltammetric growth of poly(*o*-phenylenediamine) (P*o*PD) thin films at Au electrodes in acidic, neutral, and alkaline aqueous solutions and the microetching (localized degradation) of these films for comparative examination of film porosity and stability. Some new insights into the electrochemical properties, porosity, and degradability of P*o*PD films are obtained, including a novel explanation (precipitation/dissolution of poorly soluble phenazinehydrine charge-transfer complexes) on the unusual PQCI responses observed at negative potentials in the first several potential cycles during the cyclic voltammetric growth of P*o*PD in acidic and neutral solutions and the novel EQCM quantification for the two possible structures in as-prepared P*o*PD grown from neutral and alkaline aqueous solutions. In addition, a new protocol of dynamically electrodepositing silver microwires is proposed for examining the mass-sensitivity distribution on the PQC surface.

2. Experimental Section

2.1. Instrumentation and Reagents. Figure 1 illustrates the experimental setup used in this work. The SECM/PQCI combination allowed fast and simultaneous acquisitions of the PQC electroacoustic admittance via a HP4395A impedance analyzer and of the electrochemical information via a CHI900A scanning electrochemical microscope (CH Instruments Co., U.S.A.). The CHI900A instrument consists of three Burleigh IW701-00 Inchworm motors with a maximum traveling distance of 25 mm at a 4-nm resolution, a Burleigh TS-100 three-dimensional translation stage, and a bipotentiostat. The conductance (G) and susceptance (B) data of the PQC resonance were recorded synchronously via a HP-IB interface card for Windows 3.1/NT/95 on the HP4395A equipped with a HP43961A impedance test adapter and a HP16092A test fixture, controlled by a user-written Visual Basic (VB) 5.0 program. The measurement was generally performed under conditions of 61 or 101 points, a frequency span of 30 kHz covering the PQC resonant frequency, an IF BW value of 10 kHz, and a source-power value

of 0.5 dBm. Real-time acquisitions of equivalent circuit parameters (ECPs) at an ~0.7-s (61 points) or 1.1-s (101 points) time interval could be achieved also with the same VB 5.0 program through fitting each group of *G* and *B* data to the BVD circuit. Although the apparent frequency resolution here was rather poor (61 or 101 points across 30 kHz), the random noise (fluctuation) of the fitted frequency for a stable experimental system was still as good as within ±1 Hz. The much more improved frequency precision here should come from the nonlinear least-squares fitting used, as also reported by others that the nonlinear fitting can produce much more stable and precise values.[21] Certainly, more points selected will bring about PQCI data with improved precision to some extent, but the time resolution is significantly reduced.[21] It is worth pointing out that no systematic errors were found in the data acquisition here when compared with 401 points or more selected.[21]

AT-cut 9-MHz piezoelectric quartz crystals of 12.5-mm crystal diameter were used in the experiments. The PQC was sealed on the bottom of a poly(methyl methacrylate) electrolytic cell using 704 silicon rubber adhesive. The gold electrode of 6.0-mm diameter on one side of the PQC was placed in a test solution, connected to the ground terminal of the HP16092A test fixture and used as the substrate electrode (SE) of the scanning electrochemical microscope. The Au electrode on the other side of the PQC was placed in air and served only as the connection electrode to the nonground terminal of the HP16092A test fixture. The reference electrode (RE) was a KCl-saturated calomel electrode (SCE) with a supporting electrolyte salt bridge, and all potentials in this work are referenced to it. A carbon rod served as the counter electrode (CE). The platinum microelectrode with a 25-μm electrode diameter and an ~140-μm glass-tip diameter, acting as the tip electrode (TE) of the scanning electrochemical microscope, was purchased from CH Instruments Co., U.S.A. The scanning electron microscopy (SEM) pictures were taken on a Hitachi S-570 scanning electron microscope. All chemicals were analytical grade or better. Doubly distilled water and freshly prepared solutions were used throughout. The test solutions were deareated by passing a stream of pure nitrogen for at least 20 min prior to experiments. All experiments were carried out at room temperature (20 ± 2 °C).

2.2. Procedures. The surface of the gold electrode was treated generally by washing it with 1 mol/L HNO_3 for 10 s and then with doubly distilled water. The treated electrode was then scanned between 0 and 1.5 V versus SCE in 0.20 mol/L $HClO_4$ at 50 mV/s for sufficient cycles to obtain reproducible cyclic voltammograms.[22]

For the measurements of the effects of vertical and lateral tip movements and localized density/viscosity modulation on the PQCI responses, we used 1.0 mol/L aqueous Na_2SO_4 containing 0, 1, and 100 mmol/L $K_4Fe(CN)_6$, respectively. Before the *x*-, *y*-, and *z*-movements of the tip, calibrations of the tilt of the quartz crystal plate in the *x*- and *y*-directions relative to the tip's coordinate system, the origin of the tip's coordinate system in the center of the gold excitation electrode on the quartz crystal plate, and the *z*-distance were performed as reported by Kwak and Bard.[48]

Chemical-lens-focused silver deposition reported by Hess et al. was conducted in an aqueous electrolyte containing 0.15 mol/L $AgNO_3$, 0.50 mol/L $NH_3 \cdot H_2O$, 0.50 mol/L $NaNO_2$, and 0.50 mol/L $NaNO_3$,[46] with the tip as the working electrode and the EQCM gold electrode as the counter electrode.

Poly(*o*-phenylenediamine) (P*o*PD) films were grown via potential cycling in acidic, neutral, and alkaline aqueous solutions, respectively; see related text and figure captions below

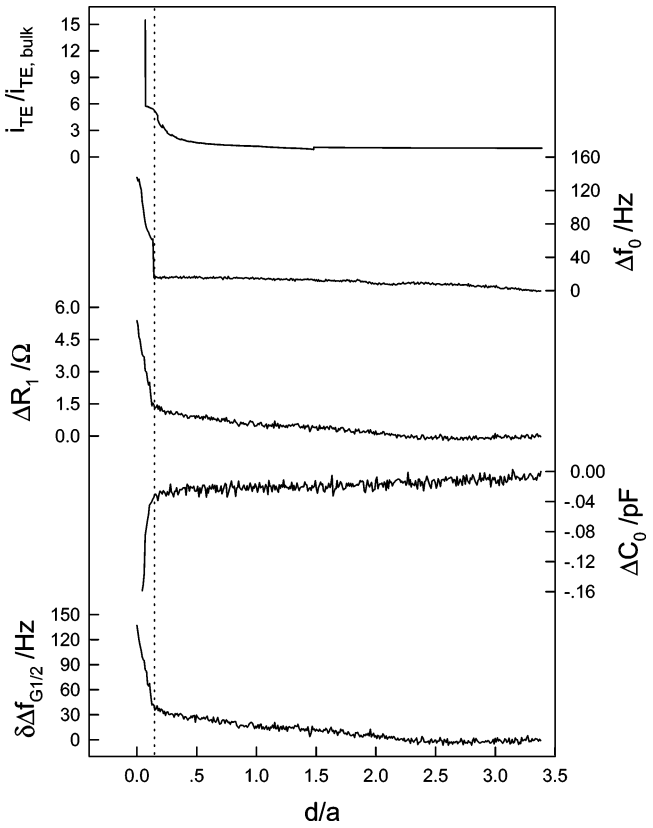

Figure 2. Responses of PQCI parameters and normalized tip current during the approach of a 25-μm Pt tip to the EQCM surface in 0.10 mol/L $K_4Fe(CN)_6$ + 1.0 mol/L Na_2SO_4. E_{TE} = 0.5 V, E_{SE} = 0 V vs SCE, a = 25 μm, and tip movement at 0.2 μm/s.

for the polymerization conditions. To evaluate the porosity of the prepared P*o*PD films, the "wet" ($\Delta f_{0w} = f_{0w2} - f_{0w1}$) and "dry" ($\Delta f_{0d} = f_{0d2} - f_{0d1}$) frequency shifts after *o*-phenylenediamine (*o*-PD) polymerization were measured as follows.[25] Before *o*-PD polymerization, the stable frequencies of the 9-MHz crystal in air and in the polymerization solution were recorded as f_{0d1} and f_{0w1}, respectively. After the polymerization, the stable frequency in the solution after potentiostatically removing the ions possibly doped into the film was recorded as f_{0w2}. The electrode was then rinsed with sufficient distilled water and dried via a stream of clean air. The stable frequency in air was recorded as f_{0d2}.

The microetching of P*o*PD films was performed in 0.10 mol/L aqueous H_2SO_4, with the EQCM gold electrode as the working electrode and the platinum microelectrode as the counter electrode. For comparison, P*o*PD films of a −1.4-kHz frequency shift were used.

3. Results and Discussion

3.1. Effects of Vertical and Lateral Tip Movements on EQCM Responses. Figure 2 shows the SECM approach curve and PQCI responses in 1.0 mol/L aqueous Na_2SO_4 containing 0.10 mol/L $K_4Fe(CN)_6$. Here, we did not find that Δf_0, ΔR_1, $\delta\Delta f_{G1/2}$, and ΔC_0 alternated periodically with the tip's approaching to the QCM surface, and even when the tip entered into the feedback area when a current increase was seen, their changes were still very small, demonstrating that the longitudinal wave effect on the QCM responses was negligible for the small tip used here.[46,49] Even when the gap between the tip and the QCM surface was slightly larger than or equivalent to the effective decay length for the QCM shear wave ($\delta \approx 0.188$ μm for a

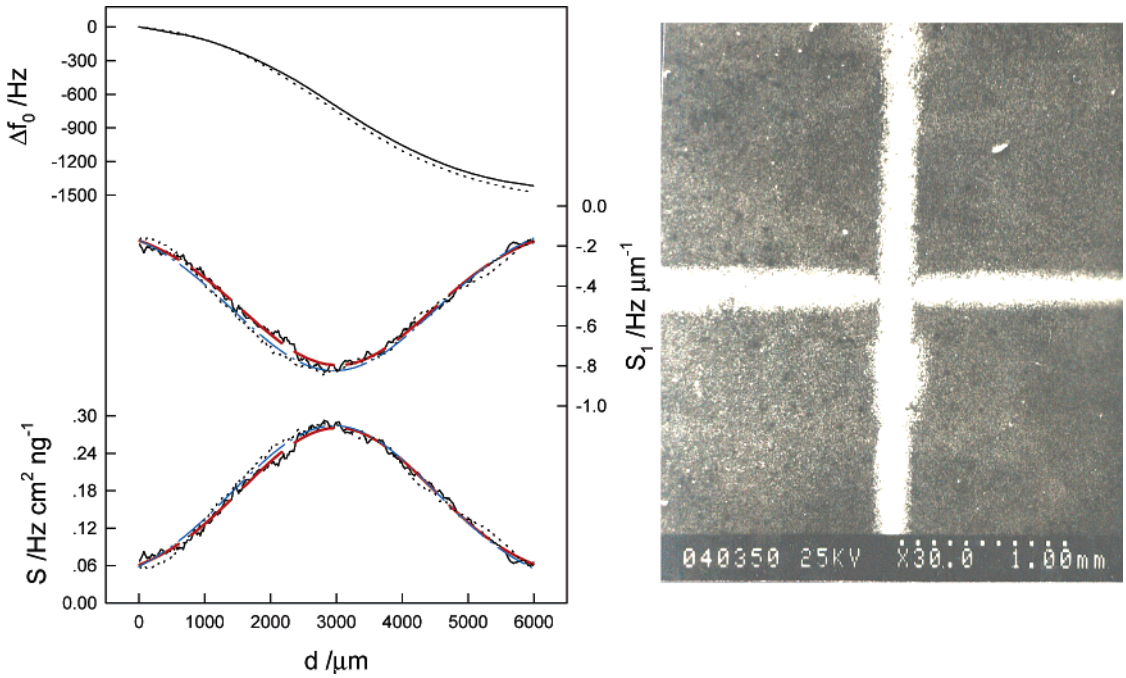

Figure 3. Δf_0, $\Delta f_0/\Delta d$ (S_1), and localized mass sensitivity per unit area (S) as a function of the tip lateral displacement (left). *y*-direction: solid line (experimental); broken line (fitted Gaussian curve). *x*-direction: dashed line (experimental); dotted line (fitted Gaussian curve). The right part of the figure shows the SEM picture for the silver microwires deposited in the *x*- and *y*-directions. See text for details.

9-MHz crystal in water),[17,49] no significant frequency decrease (increase) and resistance increase (decrease) were simultaneously observed, indicating that the electrolysis-induced viscous effect was minor here too.[23] Further perpendicular movement of the tip caused sudden and significant increases in f_0, R_1, and $\delta\Delta f_{G1/2}$ and a decrease in C_0, indicating a physical contact of the tip with the QCM surface. The notable increase in f_0 should result from the effective increases in the restoring force on crystal displacement,[44,50] and the responses of R_1, $\delta\Delta f_{G1/2}$, and C_0 observed here may reflect significant increases in the resonance-energy dissipation after the tip−QCM touch. Meanwhile, after a very slow increase, the current of the microelectrode increased explosively when the electrode tip touched the QCM surface. This is most likely because the glass of the tip contacted with the crystal electrode at first, and then, the Pt microelectrode followed, as a result of the slight tilt of the tip against the substrate.

We also examined the lateral tip movement at various vertical distances (15, 25, 225, 425, and 2250 μm) over the Au substrate on the QCM responses in 1.0 mol/L aqueous Na_2SO_4 containing 0, 1, and 100 mmol/L $K_4Fe(CN)_6$, respectively, and found in all cases that the Δf_0 (ΔR_1) responses were random and within $\pm$10 Hz ($\pm$1 Ω) during tip movements in both the *x*- and *y*-directions.

3.2. Distribution of Mass Sensitivity. Previous measurements of the radial mass sensitivity of the EQCM were performed when the tip was immobile.[41,44,46] In this work, we introduce a dynamic silver-wire deposition protocol for the first time to examine the EQCM mass sensitivity along the *x*- and *y*-axes. Experimentally, chemical-lens-focused silver deposition was performed;[46] namely, the 25-μm microelectrode was scanned at a uniform speed of 15 μm/s and a vertical tip−substrate distance of 20 μm, and a tip potential of 1.2 V versus the QCM electrode was applied. The silver wires thus deposited had an almost uniform width of ~230 μm, as shown in Figure 3 (right) via the SEM picture, and consisted of randomly distributed silver particles (~1−3-μm size). The PQCI parameters were simultaneously recorded during the deposition. The frequency response, the lateral distribution of the frequency response ($S_1 = \Delta f_0/\Delta d$), and localized mass sensitivity per unit area (S) are shown in Figure 3 (left), while the R_1, C_0, and $\delta\Delta f_{G1/2}$ responses were very small (e.g., within 1 Ω for ΔR_1) and are not shown. The charge consumed during the potentiostatic dissolution of each silver wire in the same solution was measured by integration of the *i* versus *t* curve, giving 1.385 and 1.322 mC (equivalent to 1550 and 1480 ng of the Ag deposits) for the *x*- and *y*-silver wires, respectively. By combining the QCM frequency change with the apparent area of the silver wire, the localized mass sensitivity (S) can be obtained as follows, by fitting the experimental data to the Gaussian equation

$$S_x = 0.016\,73 + 0.2673\,\exp[-2(x - 2964)^2/3076^2] \quad (3)$$

$$S_y = 0.032\,66 + 0.2481\,\exp[-2(y - 3013)^2/2889^2] \quad (4)$$

The quality of the curve fits was determined using the standard residual error of the regression given by

$$S_r = \sqrt{\frac{\sum_{i=1}^{n}(y_{i,\mathrm{data}} - y_{i,\mathrm{fit}})^2}{n-2}} \quad (5)$$

and the regression coefficient given by

$$R_{\mathrm{corr}} = \frac{\sum_{i=1}^{n}(y_{i,\mathrm{data}} - \bar{y})^2 - \sum_{i=1}^{n}(y_{i,\mathrm{data}} - y_{i,\mathrm{fit}})^2}{\sum_{i=1}^{n}(y_{i,\mathrm{data}} - \bar{y})^2} \quad (6)$$

The curve fitting resulted in residual error values of $S_{rx} = 0.0194$ and $S_{ry} = 0.0363$, with regression coefficient values of $R_{\mathrm{corr}\text{-}x} = 0.9532$ and $R_{\mathrm{corr}\text{-}y} = 0.9716$, respectively.

Integration of the sensitivity curve (S) yields the integral sensitivity values along the x- and y-directions, $C_{fx} = 0.179$ Hz cm^2 ng^{-1} and $C_{fy} = 0.176$ Hz cm^2 ng^{-1}, which differ from the mass-sensitivity value predicted by the Sauerbrey equation, $C_f = 0.183$ Hz cm^2 ng^{-1}, only by -2.2 and -3.8%, respectively, demonstrating that the dynamic silver-wire deposition protocol is feasible for the examination of the mass-sensitivity distribution on the QCM surface. In addition, drawing of a silver microwire required only 400 s here for the 15-μm/s rate of tip movement over 6 mm of electrode diameter; if a radial resolution of 5°, corresponding to 36 microwires and 4 h in total, is sufficient to complete spatially well resolved mass-sensitivity mapping on the whole QCM electrode ($2 \times 180°$), the present method is thus anticipated to be a faster method than the previously reported one.[46]

3.3. Electropolymerization of PoPD Films on EQCM Au Electrodes. Cyclic voltammetric growth of PoPD films was conducted in four solutions, acidic (A, 0.20 mol/L H_2SO_4 + 0.10 mol/L Na_2SO_4; B, 0.10 mol/L H_2SO_4 + 0.20 mol/L Na_2SO_4), neutral (C, 0.10 mol/L PBS + 0.20 mol/L Na_2SO_4, pH 7.2), and alkaline (D, 0.20 mol/L NaOH + 0.20 mol/L Na_2SO_4) aqueous solutions, involving two potential-sweep ranges, -0.4 to 0.9 (I) and 0 to 0.9 (II) V versus SCE.

In 0.20 mol/L H_2SO_4 + 0.10 mol/L Na_2SO_4 over potential range I (A-I), as shown in Figure 4 via panel A-I, a large monomer-oxidation peak (designated as O_1) appeared at ~0.70 V versus SCE during the first positive sweep.[51,52] In the following two potential-sweep segments, two new couples of redox current peaks, R_2/O_2 peaking at ~ -0.10/-0.06 V and R_3/O_3 peaking at -0.18/-0.16 V versus SCE, were observed. Peak O_1 shifted negatively and was decreased substantially in the second cycle and then gradually from the third cycle on (note the deliberate minification of the currents in the first positive potential sweep here for clarity of current traces in all cycles shown), suggesting the depletion of the monomer near the electrode surface and the loss of electrode-surface activity when covered with the polymer film, and that the oligomers were oxidized at a potential lower than that of the monomers.[53] With the increase in the number of potential cycles, the reduction peak R_2 increased notably, while the current peaks R_3 and O_2 decreased significantly.

As expected for a normal electropolymerization process, the monomer/oligomer oxidation near peak O_1 was accompanied with an f_0 decrease, and simultaneously, the changes in R_1, C_0, and $\delta\Delta f_{G1/2}$ were relatively minor. Interestingly, large and unusual responses in all Δf_0, ΔR_1, ΔC_0, and $\delta\Delta f_{G1/2}$ parameters were observed at negative potentials in the first several cycles, and they became smaller and smaller during potential cycling. Dai et al. also found similar phenomena during PoPD growth in several H_2SO_4 media via measurements of EQCM resonant frequency and admittance amplitude.[52] In this work, PQCI analyses during PoPD growth may allow us to discuss more on these interesting phenomena in a wider pH range. On the basis of the following experiments and consideration, we may reasonably explain the unusual PQCI responses as being due to the oligomer-related precipitation/dissolution. (1) The unusual PQCI responses disappeared when the solution was stirred in the first negative potential sweep from 0.8 to 0.3 V versus SCE. (2) Under identical conditions, a similar phenomenon was not observed during the cyclic voltammetric polymerization of aniline or potential cycling in an *o*-PD-free blank solution. (3) When a Au-foil electrode with an area of ~0.5 cm^2 (held at 0.8 V vs SCE) was placed above a bare QCM Au electrode whose potential was cyclically swept between 0 and -0.4 V versus SCE, with a gap of 0.2 mm between the two electrodes, similarly unusual PQCI responses were observed. (4) The current efficiency for PoPD growth during *o*-PD oxidation is calculated to be ~4% here, according to published procedures,[52] indicating that only a very small portion of the oxidation current consumed resulted in polymer formation, and the majority of it was consumed via the oxidation of the monomers to produce the cation radicals and oligomers, as also suggested by others.[52−55]

Unusual responses of all Δf_0, ΔR_1, ΔC_0, and $\delta\Delta f_{G1/2}$ parameters were also observed at negative potentials in 0.10 mol/L H_2SO_4 + 0.20 mol/L Na_2SO_4 (B-I) and 0.10 mol/L PBS + 0.20 mol/L Na_2SO_4 (C-I), with smaller amplitude at a higher pH, as shown in Figure 4 via panels B-I and C-I, with the responses of Δf_0 and ΔR_1 plotted as examples. The $\Delta f_0/\Delta R_1$ and $\Delta f_0/\delta\Delta f_{G1/2}$ values corresponding to all oligomer-related precipitation/dissolution processes at negative potentials (cases A-I, B-I, and C-I) were $\sim -13 \pm 2$ Hz Ω^{-1} and $\sim -0.60 \pm 0.1$, being very close to the theoretical values of -10 Hz Ω^{-1} and -0.50 for a net viscous effect on the 9-MHz PQC resonance, suggesting that the aggregation of insoluble substances near the QCM surface acted as a viscous and nonrigid loading, and thus accurate quantitative estimation of the net mass of the viscous deposits on the electrode is difficult via the Sauerbrey equation. The change in C_0 should reflect the dielectric change between the two EQCM oscillation electrodes, here mainly changes in the solution dielectric properties in the vicinity of the electrode surface and the electrode itself.[24,25]

It should be pointed out that the peak-type response for each PQCI parameter (especially f_0) in the case of A-I (at negative potentials during negative potential sweeps) was very insignificant or not observed at all in the cases of B-I and C-I, demonstrating the complexity of related processes. When we held the potential of the EQCM Au electrode at -0.4 V versus SCE after the first potential cycle (B-I) in a separate experiment, the oligomer-related precipitates disappeared completely after ~300 s, as suggested by the 100% recovery for each PQCI parameter when compared with that at potentials just before the precipitation. However, when we disconnected the EQCM Au electrode after the first cycle (an open-circuit state), the PQCI responses due to the oligomer-related precipitation recovered very little after 800 s, and only ~40% recovery was obtained even through solution stirring. This finding suggests that the oligomer-related precipitation/dissolution here was highly dependent on the applied potential.

The mechanism behind the unusual PQCI responses is very interesting. Inzelt and Puskás recently reported that EQCM frequency decrease/increase by over 500 Hz can be observed in the reduction/reoxidation process of high-concentration phenazine during potential cycling, as a result of the precipitation/dissolution of the phenazinehydrine (quinhydrone analogue) charge-transfer complex that is well-known to be poorly soluble,[56] and the second reduction wave of phenazine is responsible for the precipitation, while the second oxidation wave during reversal anodic scan is mainly for the dissolution.[57] Here, we may also explain the unusual PQCI responses observed as being due to the precipitation of similar phenazinehydrine charge-transfer complexes formed soon after the onset of the second reduction process (R_3) of oligomers during negative potential sweeps and their complete dissolution after the second oxidation process (O_2) of oligomers during subsequent anodic scans, since oligomers of phenazine units may have formed during the oxidation of *o*-phenylenediamine. A possible mechanism for the formation of the poorly soluble charge-transfer complex during potential cycling is given in Scheme 1, through

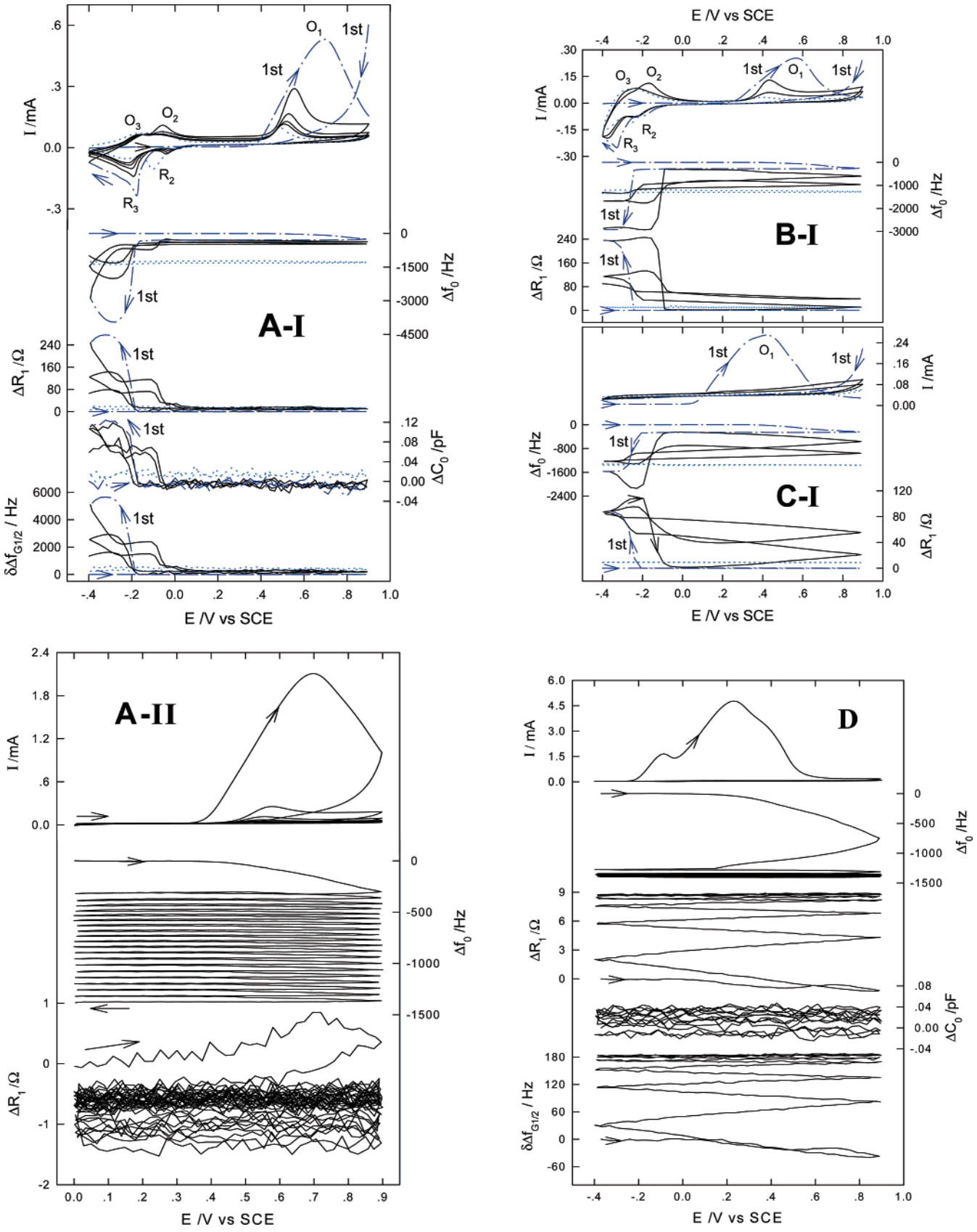

Figure 4. Simultaneous responses of current, Δf_0, and ΔR_1 (or plus ΔC_0, and $\delta\Delta f_{G1/2}$) to potential cycling in 0.10 mol/L *o*-phenylenediamine aqueous solutions containing 0.20 mol/L H_2SO_4 + 0.10 mol/L Na_2SO_4 (A-I and A-II), 0.10 mol/L H_2SO_4 + 0.20 mol/L Na_2SO_4 (B-I), 0.10 mol/L PBS + 0.20 mol/L Na_2SO_4 (C-I, pH 7.2), and 0.20 mol/L NaOH + 0.20 mol/L Na_2SO_4 (D), respectively. Scan rate: 30 mV/s. Potential ranges: I, −0.4 to 0.9 V vs SCE; II, 0−0.9 V vs SCE. For A-I, B-I and C-I, only the first three cycles and the last cycles (dashed lines) are shown for clarity of curves, and the first cycles therein are labeled as "1st" and shown in dotted lines. The current in the first positive sweep was 4× reduced in the case of A-I and 8× reduced in the cases of B-I and C-I for clarity of current traces in all cycles shown, respectively, and thus, the disconnection of current traces in A-I, B-I, and C-I at the positive potential limits is seen in the first potential cycles.

SCHEME 1: Proposed Mechanism for the Formation of the Poorly Soluble Charge-Transfer Complexes[a]

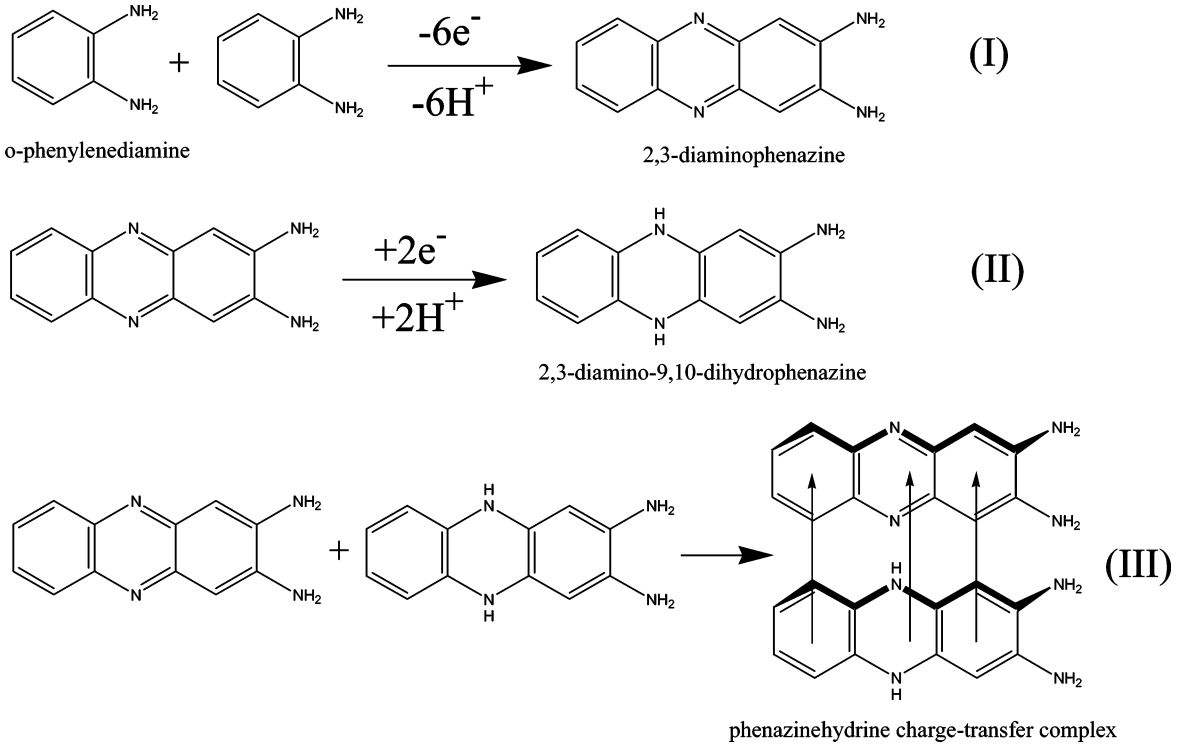

[a] The dimer (2,3-diaminophenazine) is taken here as an example of the oligomers formed during the oxidation of *o*-phenylenediamine. Note that reaction II here as a simplified one may be divided into two one-electron−one-proton steps, corresponding to the two successive reduction waves (roughly R_2 and R_3) at negative potentials in Figure 4, and the precipitation of the poorly soluble charge-transfer complex may occur soon after the formation of 2,3-diamino-9,10-dihydrophenazine at potentials near peak R_3. Note that the upward arrows indicate the direction for electron donation, and possible hydrogen bonds between the two partners for the charge-transfer complex are not shown here.

taking the dimer (2,3-diaminophenazine formed via reaction I) as an example of oligomers formed during the oxidation of *o*-phenylenediamine. This novel explanation on the unusual PQCI responses observed at negative potentials in acidic and neutral solutions is well supported by the experimental finding that the oligomer-related precipitation/dissolution was highly dependent on the applied potential, since the greatest quantity of the insoluble charge-transfer complexes should develop only at a half-reduced state of phenazine units, namely, at a molar ratio of unity of oxidized phenazine to reduced phenazine, and a less or more extent in reduction of phenazine units during negative potential sweep will decrease the quantity of insoluble charge-transfer complexes. The insoluble charge-transfer complexes can be completely dissolved after the second oxidation wave (O_2) during reversal anodic scan, as shown in Figure 4, as a result of the complete reoxidation of the reduced oligomers and thus the breakdown of the charge-transfer complexes.

For comparison, we also prepared −1.4-kHz P*o*PD films through potential cycling between 0 and 0.9 V versus SCE (potential-sweep range II) in acidic and neutral solutions, as shown in Figure 4 via panel A-II as an example. In cases A-II, B-II, and C-II, the responses of the parameters R_1, C_0, and $\delta\Delta f_{G1/2}$ were small, namely, within 3 Ω for R_1, 0.06 pF for C_0, and 60 Hz for $\Delta f_{G1/2}$. The unusual PQCI responses were not observed here, demonstrating that the precipitation of the phenazinehydrine charge-transfer complexes relies on the negative potentials that can electrochemically switch the oligomers.

Results for P*o*PD growth in the alkaline solution are shown in Figure 4 (panel D). From the second potential cycle on, the oxidation peaks became extremely small here, implying that the high pH here decreased the electroactivity and conductance of P*o*PD films due to the lack of protons required for the polymer's redox switching and doping. R_1 and $\Delta f_{G1/2}$ increased notably from the first to fourth cycle and then little during subsequent potential cycling, with maximum responses in the second cycle, and C_0 had a much smaller response due to the intrinsically smaller sensitivity and resolution of this parameter.[25] Simultaneously, f_0 decreased very largely in the first cycle (more largely than those in acidic solutions) and then slightly in the second cycle, and the frequency decreases were rather limited from the third cycle on. The observation of different PQCI responses, including the nonsynchronization of f_0 with R_1 ($\Delta f_{G1/2}$) here, probably reflects the difference in polymerization mechanisms in acidic and alkaline solutions, which may result in P*o*PD of different structures, as discussed later.

To evaluate the porosity of the prepared P*o*PD films, we also measured the wet and dry frequency shifts (Δf_{0w} and Δf_{0d}, respectively) after P*o*PD deposition. According to our previous work,[25] the ratio $R_{ee} = (\Delta f_{0w} - \Delta f_{0d})/\Delta f_{0d}$ should be an indicator of the mass percentage of electrolyte entrapped in the P*o*PD film and give us information on the film porosity. As listed in Table 1, in the cases without unusual PQCI responses, the R_{ee} values were relatively small. However, once unusual PQCI responses were observed, they became much greater, indicating a higher porosity of P*o*PD films obtained. In fact, smaller values of $|\Delta f_0/\Delta R_1|$ for the growth of P*o*PD with a −1.4-kHz frequency shift were also observed for the latter case. These observations should indicate that the precipitation/dissolution of phenazinehydrine charge-transfer complexes at negative potentials could induce less compact P*o*PD films grown from acidic and neutral aqueous solutions.

3.4. Cyclic Voltammetric Switching of As-Prepared P*o*PD Films in 0.10 mol/L Aqueous H_2SO_4—Estimation of the Molar Percentages of $-NH_2$ Groups in As-Prepared P*o*PD Films. The cyclic voltammograms of the P*o*PD-modified electrodes, after thorough washing with doubly distilled water,

TABLE 1: Results of R_{ee}, $|\Delta f_0/\Delta R_1|$ for the Growth of PoPD with a −1.4-kHz Frequency Shift, Calculated Values of the Molar Percentage of Total $-NH_2$ Groups Relative to Total Phenylenediamine Units in the PoPD Film (η_{NH2}), the Diameters of Etched Spots Calculated from QCM Data (d_{QCM}), the Tip-Diameter-Corrected Width Values of the Etched Spots from SECM Experiments (d_{SECM}), and the Average-Width Values of Etched Spots Estimated from SEM Pictures (d_{SEM})[a]

polymerization solution	potential range/V vs SCE	Δf_{0d}/Hz	Δf_{0w}/Hz	R_{ee}/%	$\lvert\Delta f_0/\Delta R_1\rvert$/Hz Ω^{-1}	η_{NH_2}/%	d_{QCM}/μm	d_{SECM}/μm	d_{SEM}/μm
0.2 M H_2SO_4 + 0.1 M Na_2SO_4 (A)	−0.4 to 0.9 (A-I)	−986	−1370	39	68.5	0	440	127	140
	0−0.9 (A-II)	−1228	−1350	10	985	0	120	53	53
0.1 M H_2SO_4 + 0.2 M Na_2SO_4 (B)	−0.4 to 0.9 (B-I)	−993	−1360	37	96.4	0	390	65	66
	0−0.9 (B-II)	−1276	−1400	9.7	1167	0	140	49	54
0.1 M PBS + 0.2 M Na_2SO_4 (C)	−0.4 to 0.9 (C-I)	−1104	−1380	25	151	8	300	62	55
	0−0.9 (C-II)	−1250	−1400	12	552	10	150	50	44
0.2 M NaOH + 0.2 M Na_2SO_4 (D)	−0.4 to 0.9	−1200	−1380	15	159	17	120	37	39

[a] The values of η_{NH_2} are estimated according to eq 7, and they are assumed to be zero, since in acidic solutions no current peaks at ~0.6 V vs SCE for $-NH_2$ oxidation were observed. d_{SEM} represents the arithmetical average value of the maximum and minimum widths of the etched spot, and d_{SECM} is the value of the bottom width of each SECM current peak shown in Figure 7 after subtracting the tip diameter.

SCHEME 2: Proposed Pathway for the Transition in Acidic Aqueous Solution from a Polyaniline-like Chain to Ladder Structure with Phenazine Units in PoPD (oxidation of $-NH_2$ Groups in PoPD)[a]

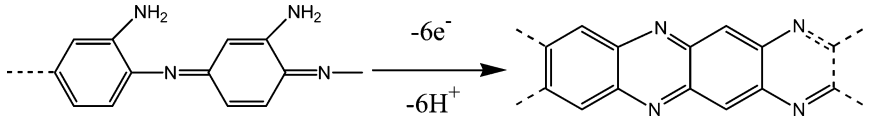

[a] Protonation and deprotonation at nitrogen atoms are not considered here.

were recorded in monomer-free 0.10 mol/L aqueous H_2SO_4, as shown in Figure 5, and some important features are summarized as follows. (1) For acidic polymerization solutions, in comparison with potential range II, the R_2 peak of PoPD in monomer-free 0.10 mol/L aqueous H_2SO_4 was shifted negatively and a new couple of redox peaks centered at ~0.3 V versus SCE (O/R) was observed for potential range I, and the height of peak O decreased significantly with potential cycling. (2) For neutral and alkaline polymerization solutions, the O_3/R_3 peaks of PoPD here became more obvious; a high oxidation peak at ~0.6 V versus SCE newly appeared for both potential ranges I and II, and its height decreased significantly with potential cycling from the first to second cycle and then decreased slower and slower. From neutral to alkaline polymerization solutions, the peaks of O_2/R_2 and O_3/R_3 in monomer-free 0.10 mol/L aqueous H_2SO_4 were shifted positively, and the oxidation peak at ~0.6 V versus SCE was also heightened. The cyclic voltammograms presented here reveal undoubtedly that the polymerization conditions, either solution pH or potential cycling range, alter significantly the electrochemical behavior of PoPD. The high oxidation peak observed at ~0.6 V versus SCE for PoPD films grown in neutral and alkaline solutions is very interesting, and at present, we may assume it as the oxidation of $-NH_2$ groups in the polymer chains, based on the following experiments and consideration. (1) The oxidation peak of $-NH_2$ groups in the *o*-phenylenediamine monomer in 0.10 mol/L aqueous H_2SO_4 was located at ~0.6 V versus SCE. (2) The addition of a few drops of $NaNO_2$ solution soon eliminated this oxidation current peak, perhaps via an azo-reaction mechanism for primary amines. (3) Potential cycling in 1.0 mmol/L phenazine + 0.10 mol/L H_2SO_4 aqueous solution did not bring about this oxidation current peak, suggesting that the possible phenazine units in PoPD should not be responsible for this oxidation peak. If this is the case, the charge consumed under the oxidation peak at ~0.6 V versus SCE (*Q*, first potential cycle) can be used to quantify the molar ratio (η_{NH_2}) of total $-NH_2$ groups relative to total phenylenediamine units in the as-prepared PoPD film grown from neutral or alkaline solution, according to the following equation

$$\eta_{NH_2} = \frac{x_{NH_2}}{x_{o\text{-PD}}} = -\frac{2.264 \times 10^{-6} f_{0g}^{\ 2} M_{o\text{-PD}} Q}{nFA\Delta f_{PoPD}} \qquad (7)$$

where x_{NH_2} is the molar quantity of the total $-NH_2$ groups in a PoPD film, $x_{o\text{-PD}}$ is the molar quantity of the total *o*-phenylenediamine units in the PoPD film that can be estimated from the Sauerbrey equation given in eq 1, $M_{o\text{-PD}}$ is the molar mass of the phenylenediamine unit in the PoPD film, *n* is the number of electrons transferred per phenylenediamine unit involved, *F* is the Faraday constant, Δf_{PoPD} is the final dry frequency shift recorded after the growth of each PoPD film, and other parameters have the same meanings as those in eq 1. The precise determination of *n* is not an easy matter here for the lack of precise knowledge on the oxidation degree of the polymer chains at present; however, we may reasonably assume it to be 3 on the basis of the transition between fully oxidized states of polyaniline-like chains and phenazine units, as depicted in Scheme 2, since the potentials involved here were near 0.6 V versus SCE.

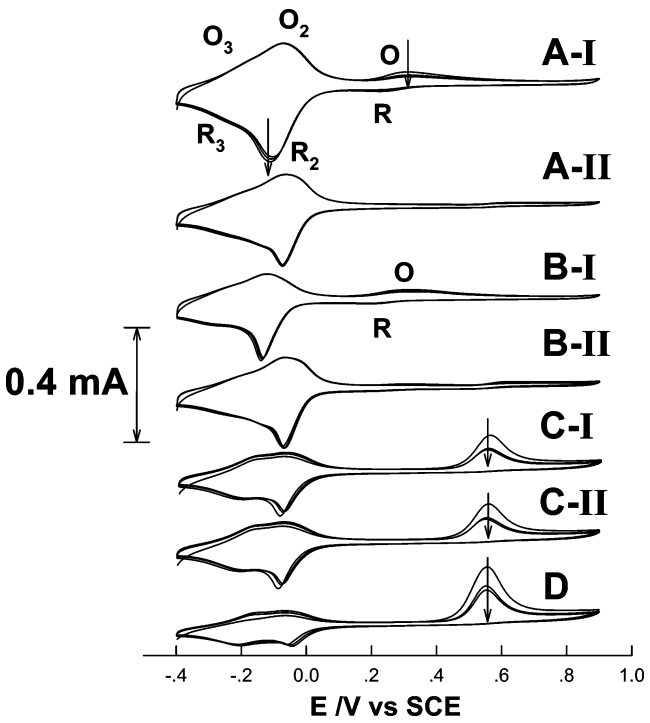

Figure 5. Cyclic voltammograms of poly(*o*-phenylenediamine) films in 0.10 mol/L aqueous H_2SO_4. Scan rate: 30 mV/s.

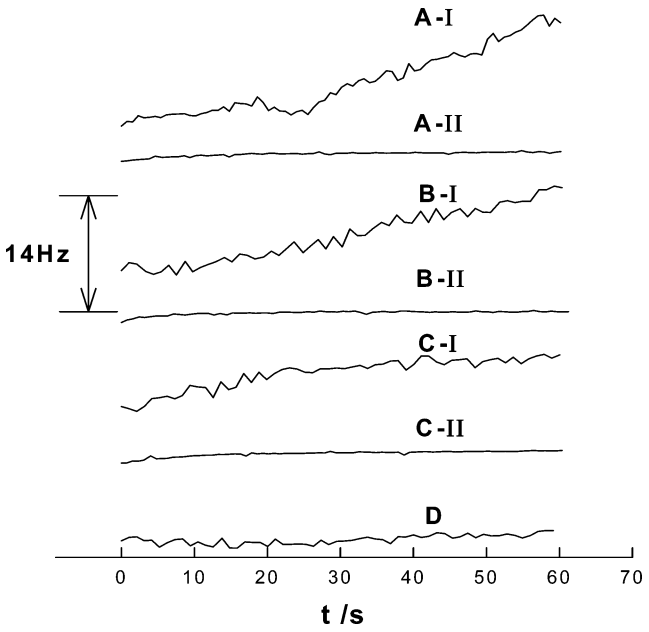

Figure 6. Δf_0 responses during microetching of P*o*PD films in 0.10 mol/L aqueous H_2SO_4. See text for details.

As listed in Table 1, for the P*o*PD film grown in the alkaline solution, the molar ratio (percentage) of the total $-NH_2$ groups reached 17%, suggesting that this P*o*PD film possesses both polyaniline-like structure and chains of phenazine units, as shown in Chart 1. Some of the $-NH_2$ groups may evolve to the phenazine structure through intramolecular cyclization during potential cycling in 0.10 mol/L aqueous H_2SO_4, as shown in Scheme 2, since the peak current for the oxidation of $-NH_2$ groups decreased with potential cycling, and the heights of O_2/R_2 and O_3/R_3 increased correspondingly. The slower and slower decrease in the peak current for $-NH_2$ oxidation after the first potential cycle may suggest that the phenazine-toward transition became slower and slower due probably to the presence of steric hindrance. The results given here are, at least, in agreement with an X-ray photoelectron spectroscopy (XPS) study by Losito et al. which showed the number of surface $-NH_2$ groups of P*o*PD film correlates positively with the pH of the polymerization solution.[15]

3.5. Microetching of P*o*PD Films. Figure 6 shows the responses of Δf_0 during the localized degradation of P*o*PD films, while the R_1, C_0, and $\delta\Delta f_{G1/2}$ responses were very small and are not shown. For comparison among experiments, the tip was held stationary at a vertical distance of 20 μm above the center of the crystal, calibrated by the described procedures, and the quartz electrode potential of 1.1 V versus the tip was applied for 60 s. As can be seen, the frequency increased with time, suggesting the loss of film mass during P*o*PD degradation. By considering the experimental QCM-center sensitivity (0.305 Hz cm^2 ng^{-1}) obtained as above via dynamically electrodepositing silver microwires and the final frequency shift of -1.4 kHz after the growth of each P*o*PD film, the diameters of etched holes (d_{QCM}) are calculated, as listed in Table 1.

Figure 7 shows the SECM profiles of the etched spots for the P*o*PD films. The spot widths (d_{SECM}), estimated from the tip-diameter-subtracted bottom width of the SECM current peaks shown in Figure 7, are listed in Table 1. Generally, d_{SECM} decreased with the pH increase for the polymerization solution, and the use of potential range II produced a smaller d_{SECM} value and thus a more compact film. The finding $d_{QCM} > d_{SECM}$ indicates that the experimental P*o*PD degradation probably occurred to some extent beyond the etching spot, leading to a larger frequency increase during P*o*PD microetching.

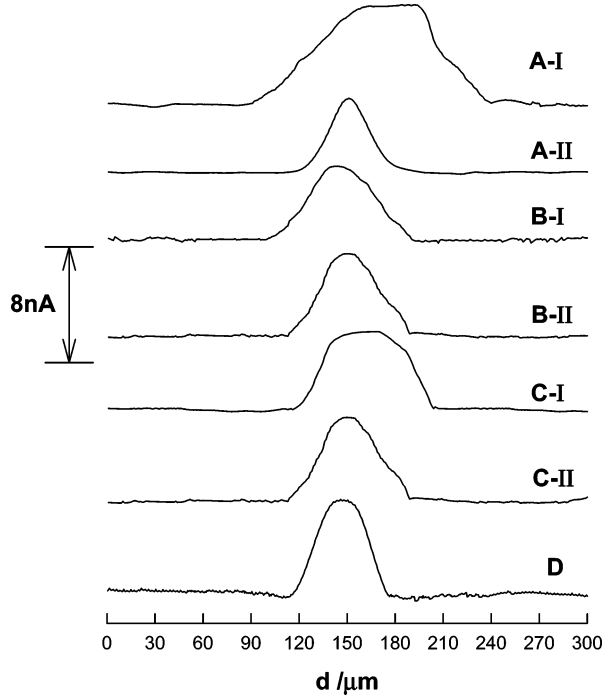

Figure 7. Current profiles obtained with a 25-μm Pt microelectrode in 2.0 mmol/L aqueous $K_4Fe(CN)_6$ containing 0.10 mol/L PBS (pH 7.2) + 0.20 mol/L Na_2SO_4 for various etched spots. $E_{TE} = 0.5$ V, $E_{SE} = 0$ V vs SCE, and tip movement along the *x*-axis at 10 μm/s.

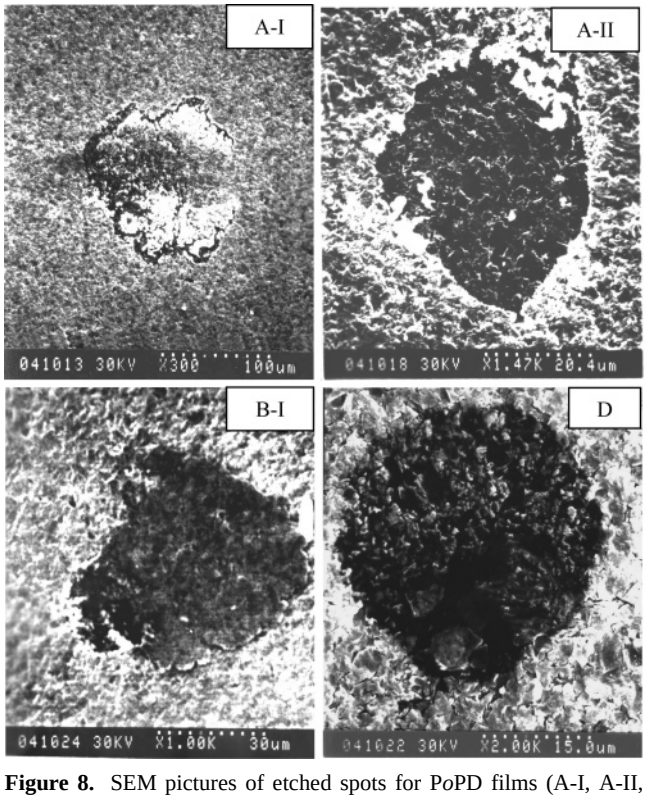

Figure 8. SEM pictures of etched spots for P*o*PD films (A-I, A-II, B-I, and D). Note that the ten-graded gauges at the bottom of the SEM pictures for A-I, A-II, B-I, and D represent 100, 20.4, 30, and 15.0 μm, respectively. See text for details.

The SECM results have been supported by SEM examinations on the etched spots, as partially shown in Figure 8. The arithmetical average values of the maximum and minimum widths of

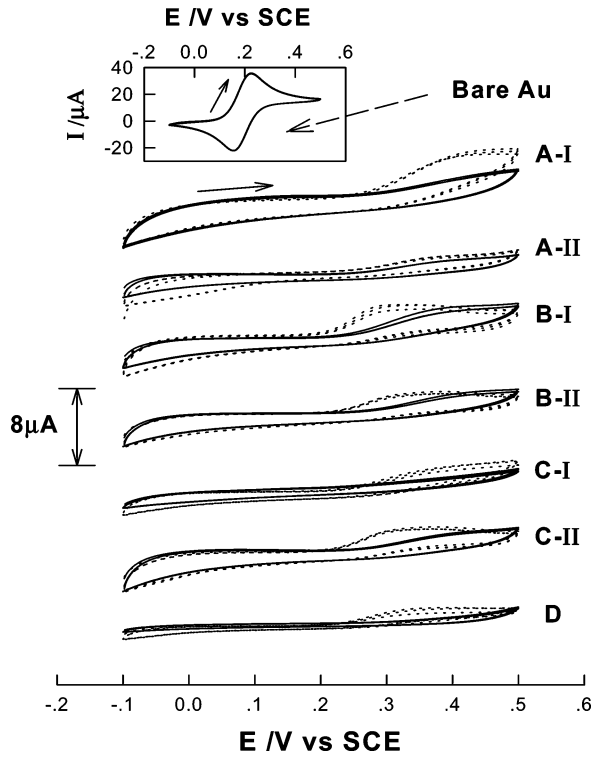

Figure 9. Cyclic voltammograms in 2.0 mmol/L aqueous $K_4Fe(CN)_6$ containing 0.10 mol/L PBS (pH 7.2) + 0.20 mol/L Na_2SO_4 before (solid lines) and after (dashed lines) microetching of P*o*PD films. Scan rate: 10 mV/s. The cyclic voltammogram at a bare Au electrode is shown for comparison.

the etched spots in the SEM pictures (d_{SEM}) are given in Table 1, which are in acceptable agreement with related d_{SECM} values.

Potential-sweep experiments in 2.0 mmol/L aqueous $K_4Fe(CN)_6$ containing 0.10 mol/L PBS + 0.20 mol/L Na_2SO_4 (pH 7.2) were conducted before and after P*o*PD films degradation, as shown in Figure 9. Very small currents were observed before degradation, demonstrating that all P*o*PD films acted as good insulators in the neutral solution. The current increases after microetching demonstrate that the tip had etched the polymer film via polymer degradation, and the larger net current increases observed for potential range I should suggest that the P*o*PD films grown in potential range II were more compact and thus more difficult to be etched experimentally.

4. Conclusions

In summary, we have demonstrated that the new SECM/PQCI combination method can provide useful multidimensional information for studying the cyclic voltammetric growth of poly(*o*-phenylenediamine) (P*o*PD) thin films at Au electrodes in acidic, neutral, and alkaline aqueous solutions and the microetching (localized degradation) of these films. Under our experimental conditions, the P*o*PD films grown between 0 and 0.90 V versus SCE (potential range II) were more compact than those grown between −0.4 and 0.9 V versus SCE (potential range I), leading to the more facile degradation for the latter P*o*PD films. The unusual PQCI responses observed at negative potentials (potential range I) in the first several potential cycles during the cyclic voltammetric growth of P*o*PD in acidic and neutral solutions have been reasonably explained as being due to the precipitation/dissolution of phenazinehydrine charge-transfer complexes developed via redox switching of the oligomers. The number of total $-NH_2$ groups in as-prepared P*o*PD was increased when higher pH values were adopted for polymerization, as quantified by considering the molar quantity of deposited polymer obtained from the EQCM data and the charge consumed under the current peak at ~0.6 V versus SCE for the oxidation of $-NH_2$ groups in P*o*PD. In addition, the *x*-, *y*-, and *z*-axis movements of a 25-μm Pt microelectrode near the PQC electrode had negligible influences on the PQCI responses, and a new protocol of dynamically electrodepositing silver microwires via the chemical-lens method was proposed for examining the mass-sensitivity distribution on the PQC surface.

Acknowledgment. This work was supported by the National Natural Science Foundation of China (20275010 and 20335020) and Hunan Province (02JJY4054), the Basic Research Special Program of the Ministry of Science and Technology of China (2003CCC00700), and the Foundation of the Ministry of Education (MOE) of China (jiaorensi [2000] 26, jiaojisi [2000] 65).

References and Notes

(1) Mederos, A.; Domínguez, S.; Hernández-Molina, R.; Sanchiz, J.; Brito, F. *Coord. Chem. Rev.* **1999**, *193*−*195*, 913.
(2) Sulimenko, T.; Stejskal, J.; Prokeš, J. *J. Colloid Interface Sci.* **2001**, *236*, 328.
(3) Garjonyte, R.; Malinauskas, A. *Sens. Actuators, B* **1999**, *56*, 85.
(4) Trojanowicz, M.; Geschke, O.; Krawczyński vel Krawczyk, T.; Cammann, K. *Sens. Actuators, B* **1995**, *28*, 191.
(5) Golabi, S. M.; Nozad, A. *J. Electroanal. Chem.* **2002**, *521*, 161.
(6) Cai, L.; Chen, H. *Sens. Actuators, B* **1999**, *55*, 14.
(7) Volkov, A.; Tourillon, G.; Lacaze, P. C.; Dubois, J. E. *J. Electroanal. Chem.* 1**980**, *116*, 279.
(8) Yano, J.; Terayama, K.; Yamasaki, S. *J. Mater. Sci.* **1996**, *31*, 4785.
(9) Malitesta, C.; Losito, I.; Zambonin, P. G. *Anal. Chem.* **1999**, *71*, 1366.
(10) Peng, H.; Zhang, J.; Nie, L.; Yao, S. Zhang, Y.; Xie, Q. *Analyst* **2001**, *126*, 189.
(11) Cheng, Z.; Wang, E.; Yang, X. *Biosens. Bioelectron.* **2001**, *161*, 79.
(12) Chiba, K.; Ohsaka, T.; Ohnuki, Y.; Oyama, N. *J. Electroanal. Chem.* **1987**, *219*, 117.
(13) Yano, J.; Nagaoka, T. *J. Electroanal. Chem.* **1996**, *410*, 213.
(14) Losito, I.; Palmisano, F.; Zambonin, P. G. *Anal. Chem.* **2003**, *75*, 4988.
(15) Losito, I.; De Giglio, E.; Cioffi, N.; Malitesta, C. *J. Mater. Chem.* **2001**, *11*, 1812.
(16) Calvo, E. J.; Etchenique, R. *J. Phys. Chem. B* **1999**, *103*, 8944.
(17) Buttry, D. A. In *Electroanalytical Chemistry*; Bard, A. J., Ed.; Marcel Dekker: New York, 1990; Vol. 17.
(18) Muramatsu, H.; Tamiya, E.; Karube, I. *Anal. Chem.* **1988**, *60*, 2142.
(19) Martin, S. J.; Granstaff, V. E.; Frye, G. C. *Anal. Chem.* **1991**, *63*, 2272.
(20) Yamaguchi, S.; Shimomura, T.; Tatsuma, T.; Oyama, N. *Anal. Chem.* **1993**, *65*, 1925.
(21) Noël, M. A.; Topart, P. A. *Anal. Chem.* **1994**, *66*, 484.
(22) Xie, Q.; Xiang, C.; Yuan, Y.; Zhang, Y.; Nie, L.; Yao, S. *J. Colloid Interface Sci.* **2003**, *262*, 107.
(23) Xie, Q.; Wang, J.; Zhou, A.; Zhang, Y.; Liu, H.; Xu, Z.; Yuan, Y.; Deng, M.; Yao, S. *Anal. Chem.* **1999**, *71*, 4649.
(24) Xie, Q.; Zhang, Y.; Yuan, Y.; Guo, Y.; Wang, X.; Yao, S. *J. Electroanal. Chem.* **2000**, *484*, 41.
(25) Xie, Q.; Zhang, Y.; Xiang, C.; Tang, J.; Li, Y.; Zhao, Q.; Yao S. *Anal. Sci.* **2001**, *17*, 613.
(26) Sauerbrey, S. *Z. Phys.* **1959**, 155, 206.
(27) Bard, A. J.; Fan, F.-R. F.; Mirkin, M. V. In *Electroanalytical Chemistry*; Bard, A. J., Ed.; Marcel Dekker: New York, 1993; Vol. 18, p 243.
(28) Arca, M.; Bard, A. J.; Horrocks, B. R.; Richards, T. C.; Treichel, D. A. *Analyst* **1994**, *119*, 719.
(29) Mirkin, M. V. *Mikrochim. Acta* **1999**, *130*, 127.
(30) Mirkin, M. V.; Horrocks, B. R. *Anal. Chim. Acta* **2000**, *406*, 119.
(31) Gabrielli, C.; Huet, F.; Keddam, M.; Rousseau, P.; Vivier, V. *J. Phys. Chem. B* **2004**, *108*, 11620.
(32) Wittstock, G.; Schuhmann, W. *Anal. Chem.* **1997**, *69*, 5059.
(33) Zhang, Z.; Yuan, Y.; Sun, P.; Su, B.; Guo, J.; Shao, Y.; Girault, H. H. *J. Phys. Chem. B* **2002**, *106*, 6713.
(34) Liu, B.; Bard, A. J. *J. Phys. Chem. B.* **2002**, *106*, 12801.

(35) Li, F.; Chen, Y.; Sun, P.; Zhang, M.; Gao, Z.; Zhan, D.; Shao, Y. *J. Phys. Chem. B* **2004**, *108*, 3295.
(36) Bard, A. J.; Fan, F.-R. F.; Pierce, D. T.; Unwin, P. R.; Wipf, D. O.; Zhou, F. *Science* **1992**, *254*, 68.
(37) Bard, A. J.; Denuault, G.; Lee, C.; Mandler, D.; Wipf, D. O. *Acc. Chem. Res.* **1990**, *23*, 357.
(38) Mandler, D.; Bard, A. J. *J. Electrochem. Soc.* **1989**, *136*, 3143.
(39) Mandler, D.; Bard, A. J. *J. Electrochem. Soc.* **1990**, *137*, 2468.
(40) Mandler, D.; Bard, A. J. *Langmuir* **1990**, *6*, 1489.
(41) Hillier, A. C.; Ward, M. D. *Anal. Chem.* **1992**, *64*, 2539.
(42) Oyama, N.; Tatsuma, T.; Yamaguchi, S.; Tsukahara, M. *Anal. Chem.* **1997**, *69*, 1023.
(43) Tatsuma, T.; Mori, k.; Oyama, N. *Anal. Sci.* **1999**, *15*, 749.
(44) Cliffel, D. E.; Bard, A. J. *Anal. Chem.* **1998**, *70*, 1993.
(45) Cliffel, D. E.; Bard, A. J.; Shinkai, S. *Anal. Chem.* **1998**, *70*, 4146.
(46) Hess, C.; Borgwarth, K.; Heinze, J. *Electrochim. Acta* **2000**, *45*, 3725.
(47) Gollas, B.; Bartlett, P. N.; Denuault, G. *Anal. Chem.* **2000**, *72*, 349.
(48) Kwak, J.; Bard, A. J. *Anal. Chem.* **1989**, *61*, 1221.
(49) Lin, Z.; Ward, M. D. *Anal. Chem.* **1995**, *67*, 685.
(50) Martin, B. A.; Hager, H. E. *J. Appl. Phys.* **1989**, *65*, 2627.
(51) Martinusz, K.; Czirok, E.; Inzelt, G. *J. Electroanal. Chem.* **1994**, *379*, 437.
(52) Dai, H.; Wu, Q.; Sun, S.; Shiu, K. *J. Electroanal. Chem.* **1998**, *456*, 47.
(53) Barbero, C.; Silber, J. J.; Sereno, L. *J. Electroanal. Chem.* **1989**, *263*, 333.
(54) Zotti, G.; Cattarin, S.; Comisso, N. *J. Electroanal. Chem.* **1988**, *239*, 387.
(55) Martinusz, K.; Inzelt, G.; Horanyi, G. *J. Electroanal. Chem.* **1995**, *395*, 293.
(56) Ramage, G. R.; Lundquist, J. K. In *Chemistry of Carbon Compounds, Part B, Heterocyclic Compounds*; Rodd, E. H., Ed.; Elsevier: Amsterdam, London, 1959; Vol. 6, pp 1374 and 1386.
(57) Inzelt, G.; Puskás, Z. *Electrochim. Acta* **2004**, *49*, 1969.